Efficient Mn recovery and as removal from manganese slag: A novel approach for metal recovery and decontamination

Separation and Purification Technology 361 (2025) 131265

Contents lists available at ScienceDirect

Separation and Purification Technology

journal homepage: www.elsevier.com/locate/seppur

Efficient Mn Recovery and As Removal from Manganese Slag: A Novel Approach for Metal Recovery and Decontamination

Jinfeng Tang [a,b], Qian Feng [a], Xiangqin Peng [c], Lizhi Tong [c,*], Jianzhao Wu [a], Xinmei Lin [a], Lezhang Wei [a,*], Minhua Su [a], Kaimin Shih [d], Małgorzata Szlachta [e], Junhua Xu [f,*]

[a] Linköping University - Guangzhou University Research Center on Urban Sustainable Development, School of Environmental Science and Engineering, Guangzhou University, Guangzhou 510006, China
[b] Nuclear Chemistry and Industrial Material Recycling, Department of Chemistry and Chemical Engineering, Chalmers University of Technology, 412 96, Gothenburg, Sweden
[c] National Key Laboratory of Water Environmental Simulation and Pollution Control, South China Institute of Environmental Sciences, Ministry of Ecology and Environment (MEE), Guangzhou 510655, China
[d] Department of Civil Engineering, the University of Hong Kong, Hong Kong SAR, China
[e] Faculty of Engineering and Natural Sciences, Tampere University, P.O. Box 541, FI-33104 Tampere, Finland
[f] Geological Survey of Finland, P.O. Box 96, FI-02151 Espoo, Finland

ARTICLE INFO

Keywords:
Manganese slag
Mn/As
Selective leaching
Mn extraction
As Adsorption/decontamination

ABSTRACT

Heavy metal contamination from mining slag poses severe environmental and health risks, especially evident with the challenges of Mn and As pollution in mining areas in China. To address this, we introduced a novel and efficient method integrating selective leaching, solvent extraction, and adsorption for Mn recovery and As decontamination. Utilizing their differential leaching behaviors, As and Mn were effectively and sequentially extracted. Under the optimal leaching conditions in our experiment, over 98% of As and 95% of Mn were leached from manganese waste slag. Mn-selective extraction was further augmented using di(2-ethylhexyl) phosphoric acid (D2EHPA), achieving a total yield of 93.1% from the HNO_3 leachate solution. Concurrently, a novel nano-hydroxyapatite@cobalt ferrite, HAP@$CoFe_2O_4$, was rationally designed for As removal, achieving an As removal rate of 99.8%. HAP@$CoFe_2O_4$ exhibited a relatively large saturation magnetization value, enabling its rapid separation from the reaction system by applying an external magnetic field. The implications of this study extend beyond mere technological advancements, highlighting the need for a broad spectrum of potential users to engage with this novel methodology for Mn waste slag treatment. Overall, this approach not only facilitated Mn recovery and As decontamination but also presented a promising solution for manganese waste slag in a broader spatial context.

1. Introduction

With the acceleration of global industrialization, heavy metals have been extensively discharged into the environment due to their widespread application in industries such as mining, metallurgy, chemical engineering, and electroplating [8]. This accumulation of heavy metals in soils has evolved into significant global concern [4], particularly in regions of high industrial activity. In China, mining areas, industrial zones, wastewater irrigation regions, and WEEE [32], dismantling sites are among the most severely contaminated, with arsenic (As) and manganese (Mn) being top pollutants of concern [15,31].

Heavy metal contamination not only compromises soil's ecological functions but also poses a significant threat to human health [18]. Pollutants in the soil can be absorbed by plants, subsequently migrating up the food chain and eventually affecting human health [1,29]. While manganese is an essential trace element, in excess it can be detrimental to human health [6], and excessive exposure can lead to neurotoxicity, affecting the nervous system [20]. In contrast, As is highly toxic and carcinogenic, presenting severe health risks even at low concentrations [7,25]. These health hazards underscore the urgency of addressing Mn and As contamination, particularly in heavily industrialized regions of China [2].

Previous studies on Mn and As contamination have focused on their migration mechanisms and impacts on soil ecosystems [22]. For

* Corresponding authors.
E-mail addresses: tonglizhi@scies.org (L. Tong), wlz2016@gzhu.edu.cn (L. Wei), junhua.xu@gtk.fi (J. Xu).

https://doi.org/10.1016/j.seppur.2024.131265
Received 12 October 2024; Received in revised form 8 December 2024; Accepted 22 December 2024
Available online 27 December 2024

example, elevated As levels significantly increase plant uptake, leading to heavy metal accumulation in food chains [11]. Similarly, soil microbial diversity decreases with proximity to mining areas [23]. These findings emphasize the need for effective remediation technologies tailored to the unique behaviors of Mn and As in contaminated soils [3].

Various remediation techniques for the treatment of Mn and As pollution, such as selective adsorption using biochar composites [26], advanced leaching techniques employing organic acids [17], solidification/stabilization with modified hydroxyapatite [14], and bioremediation [21,33] have been explored. These approaches have demonstrated promising results in specific scenarios, However, the principles and applicability of these techniques vary across different domains [12,28], facing challenges such as high cost, incomplete removal, or secondary pollution [10]. For instance, soil washing often struggles with balancing efficiency and environmental safety [9,16]. These limitations highlight the need for novel approaches that integrate efficiency with sustainability [30].

In this study, an integrated approach combining selective leaching, solvent extraction, and adsorption is proposed for Mn recovery and As decontamination from manganese slag. The distinct behaviors of Mn and As during the leaching process were leveraged through a novel selective leaching experimental design, enabling stepwise and efficient extraction of both elements. Subsequently, Mn recovery and As removal from water were successfully achieved through solvent extraction and adsorption, with optimization of the corresponding experimental parameters. Furthermore, a comprehensive assessment of potential impacts on relevant stakeholders was also conducted. This approach not only provided us a clearer insight into the potential real-world outcomes of our technique but also offered invaluable guidance for subsequent decision-making in future implementations.

2. Materials and experimental

To comprehensively assess the contamination status of the manganese slag site, systematic sampling of manganese slag and surrounding soil samples was conducted. The sampling method combined point selection with regional point allocation, incorporating a grid system to finely divide the landfill site into multiple 40 m × 40 m grids, ensuring that each 1,600 m^2 area contained at least one soil sampling point. This approach identified 79 unique sampling locations, resulting in the collection of 400 soil samples. Subsequently, interpolation analysis was performed using ArcGIS software, successfully generating a spatial distribution map of the contamination status at the landfill site, as shown in Fig. 1.

The concentrations of major and minor elements were measured in the soil samples (Table 1) and the target Mn waste slag samples (Table 2). The heavy metal concentrations were determined by inductively coupled plasma-optical emission spectroscopy (ICP-OES) (main elements) and inductively coupled plasma-mass spectroscopy (ICP-MS) (trace elements) after total dissolution by an external laboratory using standard accredited methods.

As can be seen in Table 1, the concentrations of As and Mn in the soil samples significantly exceeded the current national standard and provincial standard, respectively, with maximum values exceeding the limits by 9.8 and 2.7 times, respectively. Additionally, soil samples from specific points yielded slight exceedances for Pb and Co. The concentrations of other heavy metals tested were within the permissible limits at all sampling points. Consequently, As removal and Mn recovery were selected as the primary focus of this study.

Analytical-grade chemicals were employed for all parts of this study. Deionized water (>18 MΩ/cm) was used for preparing aqueous solutions. In this work, the input mass concentrations were defined as the maximum available concentrations of selected metals in the effluent.

The target Mn slag samples primarily comprise three components: leaching neutralization slag, sulfide slag, and anode mud. The composition of the leaching neutralization slag is mainly based on the

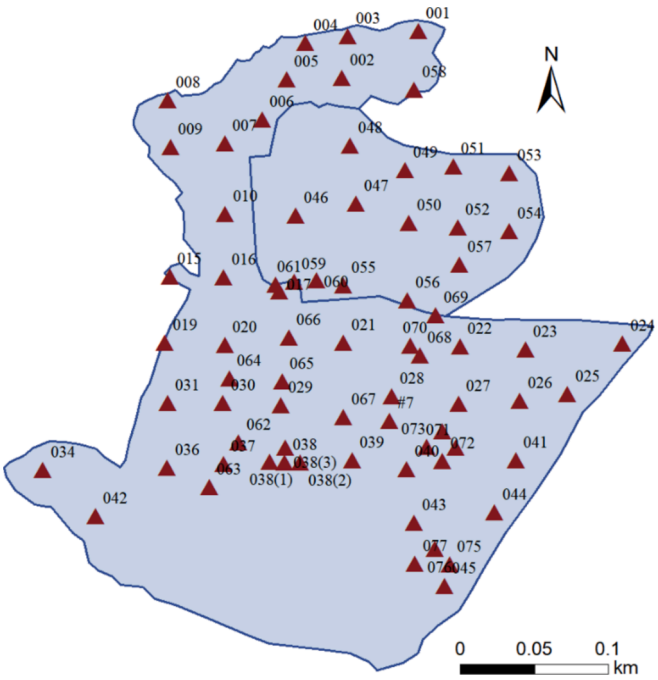

Fig. 1. Soil sampling areas and sampling points. The solid line represents the soil sampling area plotted by latitude and longitude, while the triangles indicate the sampling points.

Table 1
Heavy metal concentrations in soil samples and limit values.

Element	Meanmg/kg	Min. mg/kg	Max.mg/kg	Standard Limit mg/kg	Standard
Cr	219.0	64	2,500	2,910	DB43/T1165-2016
Mn	4,680	336	37,500*	10,000	
Zn	440	70	2,560	10,000	
As	130	15.8	590*	60	GB36600-2018
Cd	7.02	0.2	40	65	
Cr(VI)	0.22	ND	0.45	5.7	
Cu	198.0	23	2,410	18,000	
Pb	391.0	23.5	810	800	
Hg	0.38	0.03	1.44	38	
Ni	145.0	30.9	499	900	
Co	23.7	7.43	85	70	

* Indicates a pollutant whose content exceeds the risk screening value for soil contamination of development land in the national soil environmental quality standard (GB36600-2018) or the Hunan provincial standard (DB43/T1165-2016) (for Cr, Mn, and Zn).

Table 2
Element concentrations in the Mn waste slag samples. Major elements are presented as wt% and minor elements as mg/kg.

Major element	wt%	Minor element	mg/kg
Al	4.31	As	640
Ca	5.67	Cd	60
Fe	13.65	Co	110
K	0.75	Cr	80
Mg	1.43	Cu	3,500
Na	0.11	Li	100
Si	7.24	Mn	83,000
Ti	0.15	Ni	840
		Pb	1,300
		Rb	110
		Sr	140
		Zn	4,080

manganese carbonate ore and soft manganese ore provided by the project developer, which includes constituents such as $Fe(OH)_3$, $CaSO_4$, $Mg(OH)_2$, and SiO_2. Additionally, the sulfide slag mainly contains elements such as Mn, Pb, Zn, and S. On the other hand, the primary component of the anode mud is Mn.

Mn slag samples were collected, and then the samples were air-dried, homogenized, and sieved through a 100-mesh sieve to ensure uniform particle size. Approximately 500 g of the processed sample was stored in sealed polyethylene bags for subsequent experiments.

2.1. Selective leaching

The overall experimental procedure is presented in Fig. 2. In the leaching tests, a diverse set of leaching agents was employed, including sodium hydroxide (NaOH, Sigma Aldrich), hydrochloric acid (HCl, Sigma Aldrich), nitric acid (HNO_3, Sigma Aldrich), and deionized water (>18 MΩ/cm).

Leaching experiments were conducted in a 250-mL glass reactor equipped with a magnetic stirrer. the leaching agents was prepared using analytical-grade reagents and deionized water. By systematically modulating the experimental parameters, such as the concentration of the leaching agent (0.5 – 3 M), the liquid-to-solid ratio (expressed in v/w terms) (5, 10, 50 v/w), the duration of leaching (0.5 – 20 h), and the leaching temperature (20, 30 and 40 °C)under constant stirring at 300 rpm, the distinct leaching behaviors of Mn and As could be screened. After the reaction, the leachate was filtered and analyzed for metal concentrations using ICP-OES. This comprehensive analysis facilitated the identification of the most favorable conditions for achieving the sequential and selective leaching and separation of these two elements.

2.2. Mn extraction

For the solvent extraction of manganese, di(2-ethylhexyl) phosphoric acid (D2EHPA P204, 97 %, Sigma Aldrich, Germany) was employed as the extraction reagent. This reagent was utilized as received, without undergoing any further purification. Kerosene (Solvent 70, Statoil) served as the diluent. Extraction and stripping tests were conducted in 3.5 mL glass vials using an IKA Vibrax shaking machine (Germany), which operated at a frequency of 1000 vibrations per minute (vpm) at ambient temperature (20 ± 1 °C), ensuring optimal contact between the phases. Key variables, including the contact time (1 – 30 min), pH of the aqueous solution (in the range of 1.0 – 4.0), and the concentration of the extractant (0.1 – 1 mol/L), were systematically investigated. After settling, the two phases were separated using a separating funnel, and the aqueous phase was analyzed for Mn concentration using ICP-OES.

For stripping experiments, the Mn-loaded organic phase was contacted with sulfuric acid (H_2SO_4, Sigma Aldrich) under the same conditions. The stripping efficiency was calculated based on the amount of Mn transferred back to the aqueous phase.

2.3. As decontamination

Hydroxyapatite (HAP)($Ca_{10}(PO_4)_6(OH)_2$) exhibits superior metal adsorption properties [26,35]. Thus, nano-scaled HAP@$CoFe_2O_4$ was selected as the adsorbent and synthesized as reported in [24]. To thoroughly understand the adsorption capability of an adsorbent, it is crucial to examine its physical and chemical characteristics. Notably, factors such as the availability of functional groups, surface area, and porosity play significant roles in determining the efficiency of an adsorbent. To elucidate these properties for the HAP@$CoFe_2O_4$ granules, a series of analyses were conducted. Firstly, the crystal structure and phases of HAP@$CoFe_2O_4$ were characterized using X-ray diffraction (XRD) on a PANalytical PW3040/60 instrument (Netherlands). For a deeper insight into its porous nature, a sample of HAP@$CoFe_2O_4$ (approximately 0.1 g) was placed in a quartz tube and subjected to an intensive degassing process overnight at 50 μm Hg and 120 °C. Upon reweighing the degassed sample, nitrogen adsorption/desorption measurements were taken by utilizing a state-of-the-art specific surface analyzer, ASAP 2020 (Micromeritics, USA). The Brunauer–Emmett–Teller (BET) method was employed to determine the specific surface area. Furthermore, the surface morphology of HAP@$CoFe_2O_4$ was visualized by transmission electron microscopy (TEM) using a JEOL JSM-2100F instrument.

For the efficient removal of As from real wastewater, we developed and utilized hydroxyapatite nanoparticles coated with cobalt ferrite, denoted as HAP@$CoFe_2O_4$. Considering the complexity of real wastewater, with the presence of multiple metal ions, the main focus was on the ability of HAP@$CoFe_2O_4$ to selectively adsorb As, while being aware of potential competitive adsorption phenomena. The key parameters, including the contact time, pH of the solution, and adsorbent dosage, were thoroughly studied to determine their impact on As removal and to understand the selective adsorption behavior in the presence of other coexisting ions. Solutions ranging from 1.0–3.0 g/L of HAP@$CoFe_2O_4$ were evaluated to determine the effect of adsorbent dosage, solution pH,

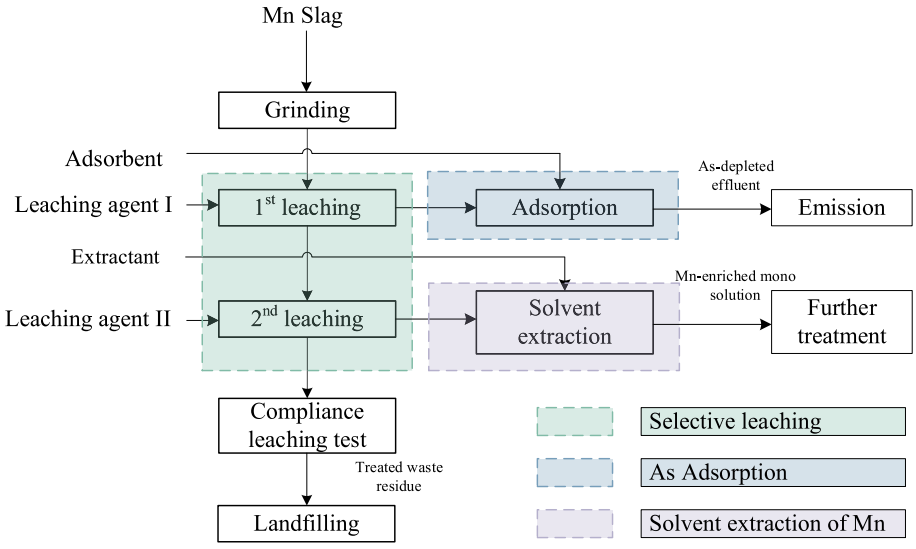

Fig. 2. Schematic diagram of the overall experimental procedure, integrating the 1st selective leaching test, 2nd leaching test, Mn extraction, and final effluent decontamination (As adsorption).

and contact time. The influence of the initial solution pH was examined in the pH range of 2.0–8.0, and pH was adjusted using HNO_3 or NaOH solutions.

3. Results and discussion

3.1. Bath leaching

3.1.1. Effect of leaching agents

As presented in Fig. 3**a**, it is evident that among all the leaching agents tested, both sodium hydroxide solution and ammonium hydroxide solution failed to leach Mn from the slag. This observation can probably be attributed to the predominant presence of Mn in its stable oxidation states within the slag, which exhibit reduced solubility in alkaline environments. Consequently, Mn leaching proved ineffective under the alkaline conditions presented by sodium hydroxide and ammonium hydroxide. In contrast, deionized water, although initially demonstrating a relatively low leaching efficiency, exhibited a progressive increase over time, achieving an efficiency of 17.6 % by 20 h. Notably, both hydrochloric acid and nitric acid solutions displayed high leaching efficiencies in shorter durations, with both surpassing a leaching rate of 39.0 % after only 4 h. Thus, an acidic environment is recommended for the efficient leaching of Mn from the slag.

The leaching behavior of As using various leaching agents is illustrated in Fig. 3**b**. From the dataset, deionized water and ammonium hydroxide exhibited no As leaching across all tested time intervals. This observation implies that the specific chemical forms of As in the Mn slag remain insoluble in neutral and weakly alkaline environments. Conversely, HCl solution initiated As leaching at an efficiency of 23.8 % at 0.5 h, reaching up to 46.8 % by 20 h. Similarly, HNO_3 solution started with a 24.9 % leaching efficiency at 0.5 h, peaking at 48.8 % by 20 h. Both acids displayed a consistent enhancement in performance with extended leaching durations. Notably, sodium hydroxide solution outperformed other agents, with a 33.3 % leaching efficiency at 0.5 h and culminating in 67.0 % leaching by 20 h. This pronounced efficiency can be ascribed to the increased solubility of specific As forms in Mn slag under alkaline conditions.

It is also evident that Mn and As demonstrate distinct leaching behaviors under acidic and alkaline conditions. It is feasible to sequentially leach Mn and As from Mn slag. Subsequently, these elements can be effectively separated, removed, and recovered. Based on the experimental findings, HCl, HNO_3 and NaOH solutions were selected for further investigation.

3.1.2. Effect of the leaching agent concentration

From Fig. 4, it can be observed that the leaching rate of As and Mn is significantly influenced by the concentration of the leaching agent. Specifically, as presented in Fig. 4**a**, with a leaching duration of 20 h, the leaching rate of As increased from 67 % to 85.5 % as the NaOH concentration increased from 0.5 M to 1.0 M. When the NaOH concentration was further increased to 3.0 M, the leaching rate reached a maximum of 93.3 %.

The systematic evaluation of Mn leaching behavior across different leaching agents and concentrations revealed a pronounced correlation between the concentration of the leaching agent and the leaching efficiency of Mn. Both HCl and HNO_3 displayed this trend.

For HCl solution in particular, as presented in Fig. 4**d**, as the concentration was increased, a marked rise in Mn leaching efficiency was observed. At the moderate concentration of 0.5 mol/L, the leaching efficiency reached 50.1 % after 20 h. However, when the concentration was doubled to 1 mol/L, the efficiency greatly increased, reaching 79.4 % by the 20-hour interval. Most notably, at the highest tested concentration of 3 mol/L, an impressive leaching efficiency was recorded, with over 95 % of Mn being successfully leached after 20 h. A similar trend was evident with HNO_3 leaching (Fig. 4**f**). At a concentration of 3 mol/L, the leaching process culminated in the extraction of almost 98.2 % of Mn by the end of 20 h.

As illustrated in Fig. 4**d and 4f**, the leaching efficiency generally increased with a prolonged leaching time, but the release of Mn and As from slag then gradually slowed down. At 20 h, the leaching process approached equilibrium. This was primarily due to the decreasing availability of easily soluble manganese compounds as the leaching progressed, leaving behind manganese minerals that are less soluble Mn compounds. Additionally, changes in reaction conditions, complex chemical reaction steps, and the diminishing effects of mass transfer and diffusion collectively contributed to the slowing rate of increase in leaching efficiency.

The experimental results demonstrated that a concentration of 3 mol/L achieved more than 95 % extraction of the target metals, indicating a very high leaching efficiency. Within the tested concentration range of the chosen leaching agents, 3 mol/L was confirmed to be the most effective choice for As and Mn leaching.

3.1.3. Effect of the L/S ratio

The relationship between the liquid-to-solid (L/S) ratio and the leaching behavior of Mn is illustrated in Fig. 5. While the variation in leaching efficiency for Mn across different L/S ratios was relatively subtle, the effect on As was more pronounced when using NaOH as the leaching agent. Specifically, at an L/S ratio of 50 with NaOH solution, the leaching efficiency of As reached 98.9 % after 20 h, indicating that over 95 % of As was extracted. This highlights the crucial role of the L/S ratio, especially under alkaline conditions, in facilitating effective As removal from manganese slag.

Although modifying the L/S ratio influenced the leaching efficiency

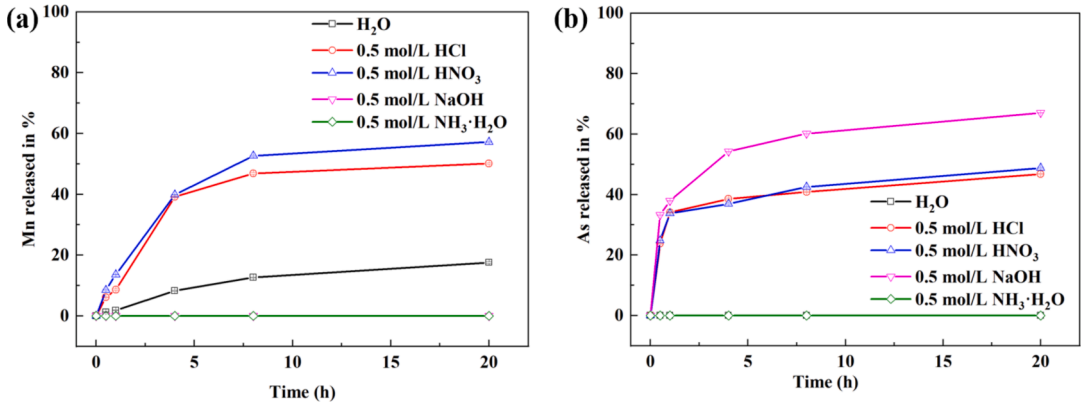

Fig. 3. Leaching behavior of (a) Mn and (b) As from Mn slag at ambient temperature with various leaching agents. L/S ratio = 10. Standard deviation based on triplicate tests.

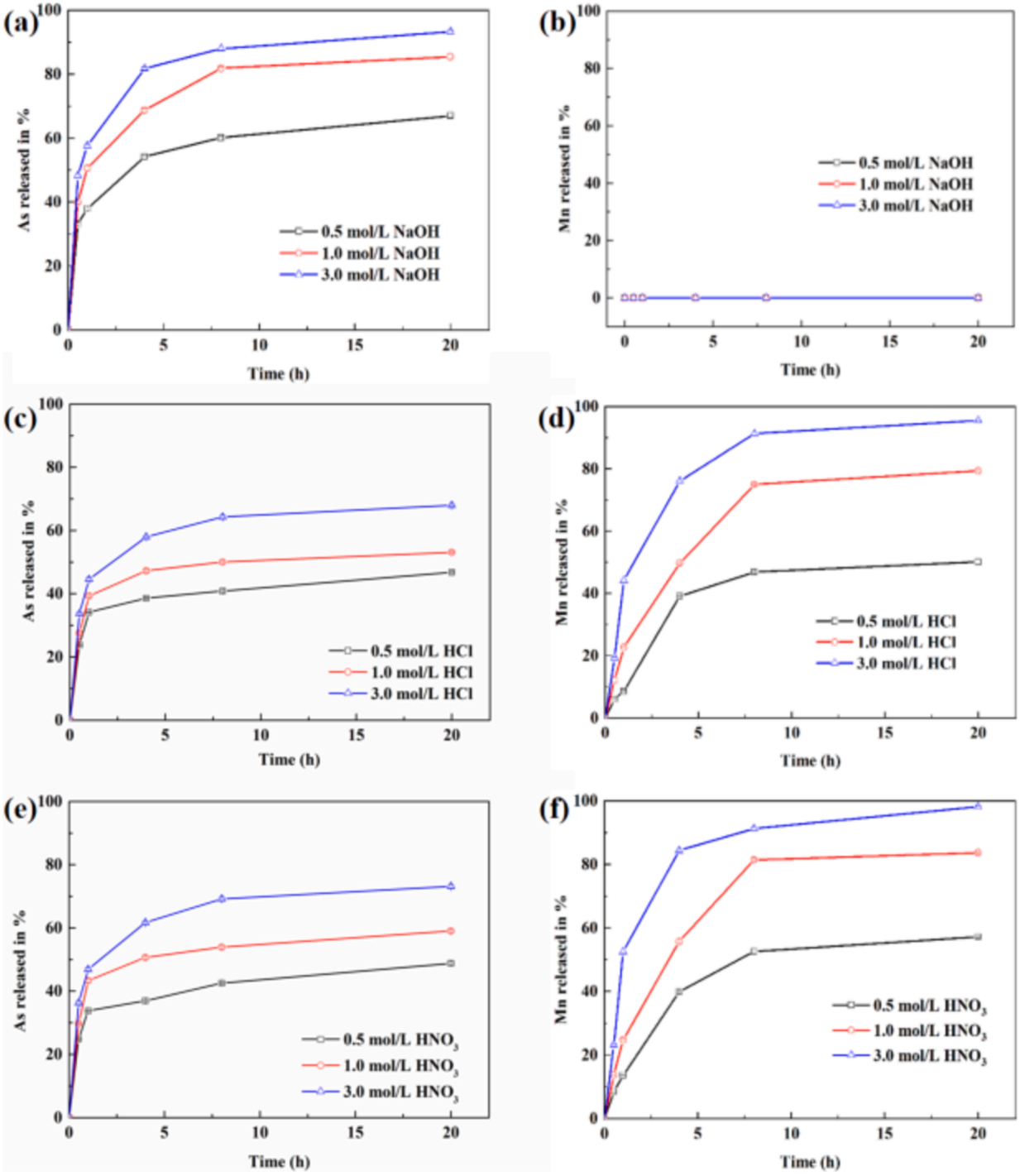

Fig. 4. Leaching behavior of As and Mn released from Mn slag using a concentration of 0.5, 1, and 3 mol/L (L/S = 10) of NaOH solution (a–b), HCl solution (c–d), and HNO_3 solution (e–f). Standard deviation based on triplicate tests.

of Mn, the overall impact on the leaching rate across different L/S ratios was not significantly pronounced. In the tests with HCl as the leaching solution, the Mn leaching rate at L/S ratios of 5, 10, and 50 was approximately 93.5 %, 95.5 %, and 95.4 %, respectively, at 20 h. With HNO_3 solution, the respective rates were approximately 95.7 %, 98.2 %, and 98.7 % for the same L/S ratios and duration. While the end leaching efficiencies were relatively similar between the different L/S ratios, it is notable that a higher L/S ratio tended to accelerate the kinetics of the leaching process, leading to a faster attainment of high leaching rates in the initial stages. This suggests that optimizing the L/S ratio can provide kinetic advantages in the leaching of Mn, even if the ultimate leaching efficiencies across different L/S ratios converge to similar values.

Additionally, a high L/S ratio can lead to an increased consumption of the leaching agent and higher subsequent treatment costs. Therefore, in practical applications, it is necessary to balance the leaching efficiency with the economic cost. Based on these considerations, the optimal L/S ratio in this study was determined to be 10.

3.1.4. Effect of the leaching temperature

The effect of temperature on the leaching behavior of As using NaOH, and of Mn using HCl and HNO_3 solutions is illustrated in Fig. 6. After a constant leaching time of 20 h, the leaching rate of As was found

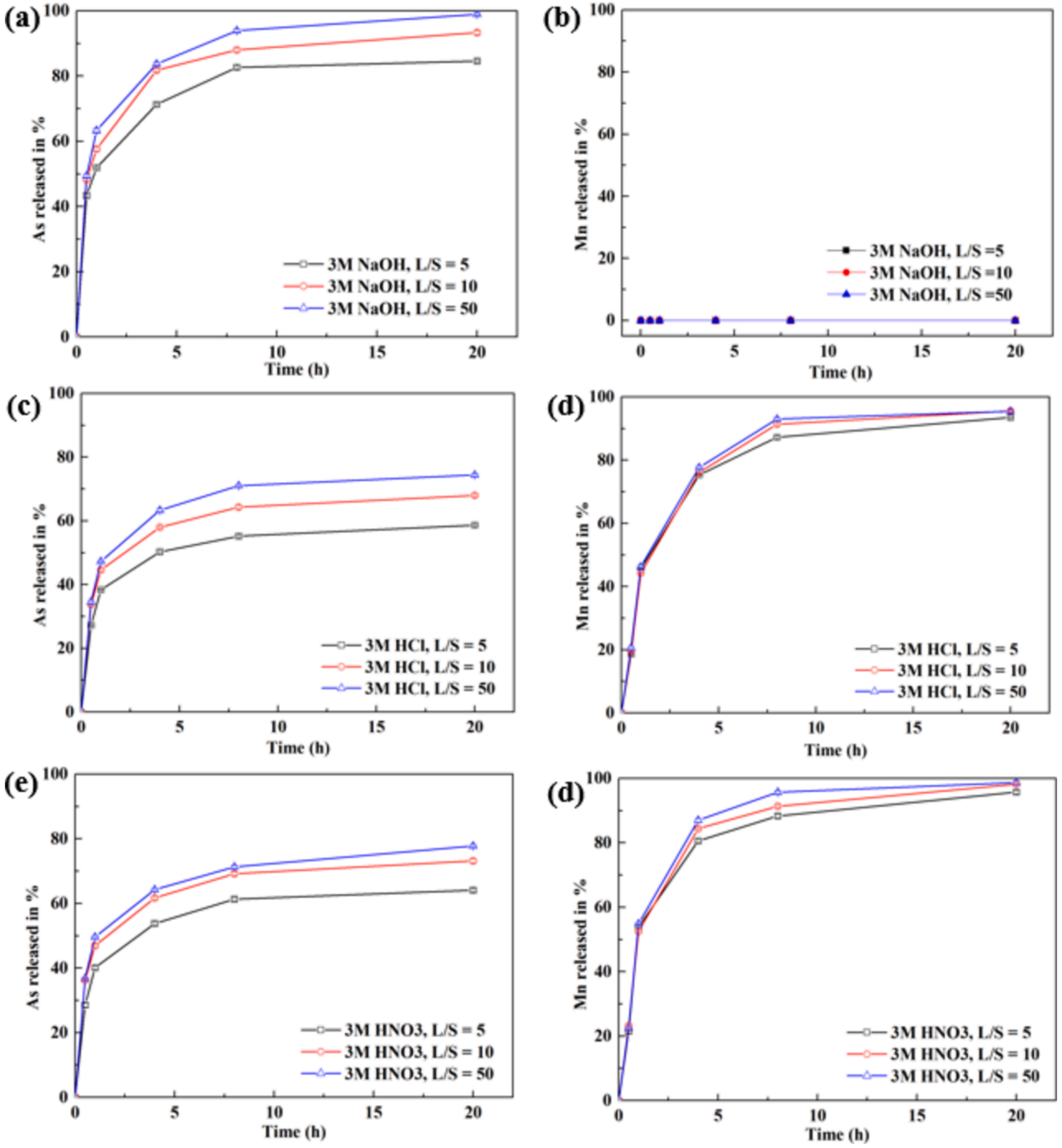

Fig. 5. Effect of the liquid–solid ratio on the As and Mn leaching rate using a 3 mol/L solution of NaOH (a–b), HCl (c–d), and HNO_3 (e–f) with different L/S ratios of 5, 10, and 50 v/w. Standard deviation based on triplicate tests.

to be 98.9 % at 20 °C, with slight increases to 99.2 % and 100 % at 30 °C and 40 °C, respectively. This indicates that while increasing the temperature has some promoting effect on the leaching rate, its impact is relatively limited during the leaching process, especially with a longer leaching duration.

Furthermore, the influence of temperature on the leaching kinetics is more pronounced. At higher temperatures, the leaching rate of As significantly accelerated. For instance, at 40 °C, the leaching rate of As rapidly increased to roughly 86 % within 5 h, whereas achieving the same leaching rate at 20 °C required 10 h. This suggests that elevating the temperature effectively speeds up the chemical reaction, enabling the leaching rate to approach high levels more rapidly in the initial stages of the experiment, thereby shortening the time to reach the leaching equilibrium.

The leaching behavior of Mn using HCl and HNO_3 solutions is illustrated in Fig. 6**b and 6c**. As depicted in Fig. 6**c**, with a leaching duration of 20 h at 20 °C, Mn approached complete leaching with a high leaching rate of 98.2 %. Upon increasing the temperature to 30 °C and 40 °C, the leaching rates of Mn slightly rose to 98.8 % and 99.6 %, respectively.

Similar results were observed for HCl leaching (Fig. 6**b**). At 20 °C, the leaching rate of Mn reached 95.4 % after 20 h. When the temperature

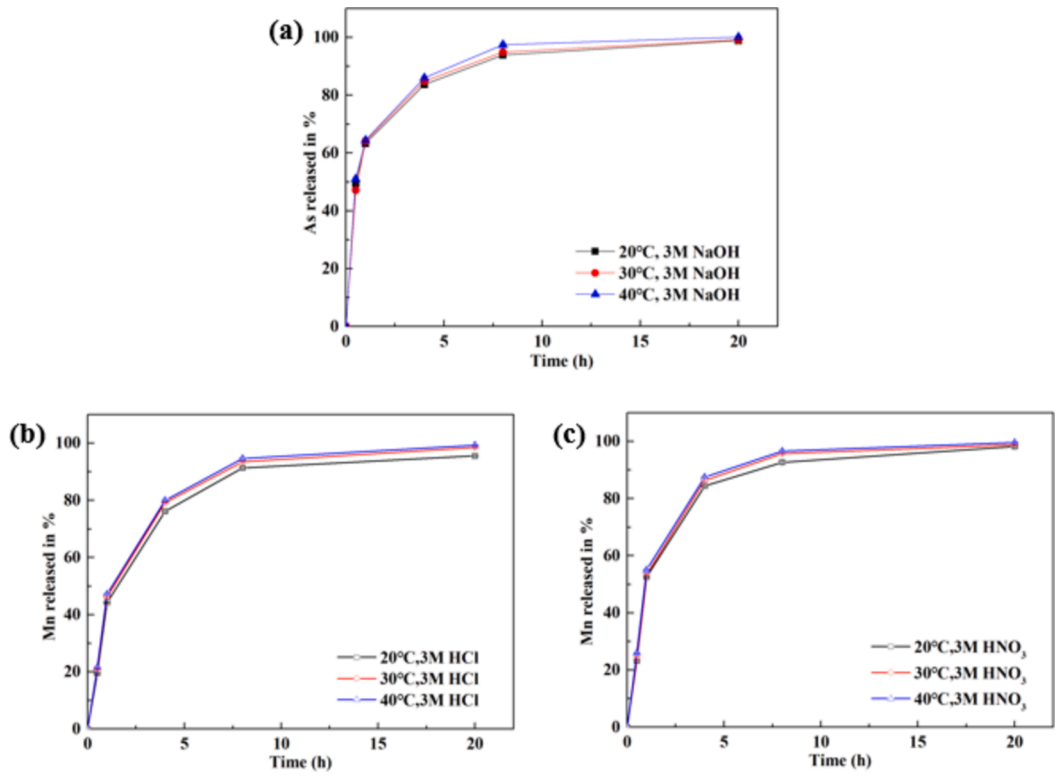

Fig. 6. Leaching behavior of As and Mn from Mn slag using a 3 mol/L solution of NaOH (a–b), HCl (c–d), and HNO_3 (e–f) at three temperatures (20 ± 1°C, 30 ± 1 °C and 40 ± 3 °C) (L/S ratio = 10). Standard deviation based on triplicate tests.

was increased to 30 °C and 40 °C, the leaching rates after the same 20-hour period increased to 98.5 % and 99.3 %, respectively. Although raising the temperature can marginally enhance the final leaching rate of Mn, the improvement across different temperatures is not significant, especially with longer leaching durations. Therefore, the findings of this study underscore the feasibility and efficiency of Mn leaching at ambient temperature.

Based on the observations above, as presented in Fig. 7, optimal leaching conditions for a two-stage selective leaching system were established.

In the first stage, targeting As leaching, a 3 mol/L NaOH solution at ambient temperature with an L/S ratio of 50 and a leaching duration of 20 h can effectively extract over 90 % of As from the manganese slag without disturbing the manganese content. The mass loss rate of the slag during As leaching using NaOH is illustrated in Fig. 8. At a concentration

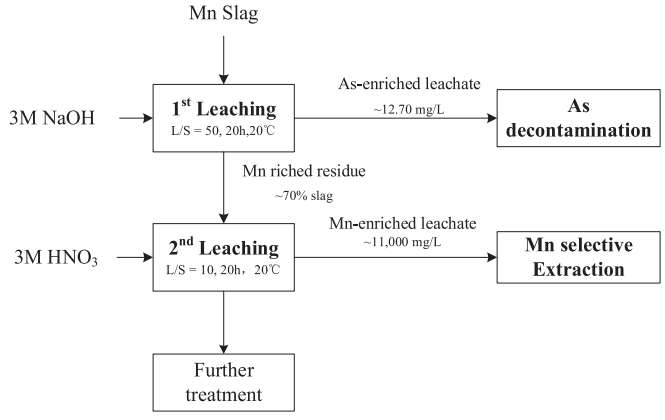

Fig. 7. Schematic diagram of the two-step leaching process to sequentially release As and Mn from manganese slag.

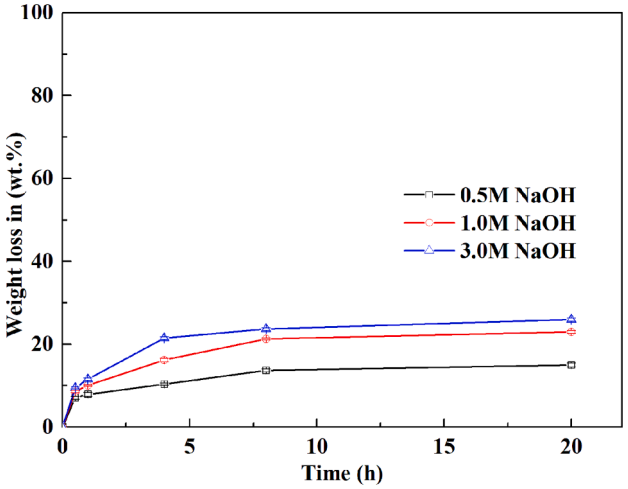

Fig. 8. Weight loss of Mn slag during leaching using NaOH solution as a leaching agent, L/S = 50, ambient temperature. Standard deviation based on triplicate tests.

of 0.5 mol/L NaOH, the mass loss rate of the slag was approximately 15 % after 20 h. When the NaOH concentration was increased to 1 mol/L, the mass loss rate rose to 23 %. Further increasing the NaOH concentration to 3 mol/L resulted in a mass loss rate of 26 %. These data clearly indicate that higher concentrations of NaOH significantly enhance the leaching efficiency of As from Mn slag.

For the second stage, Mn leaching was performed using a 3 mol/L solution of HNO_3/HCl. The conditions for this stage were set at ambient temperature with an L/S ratio of 10 and a leaching period of 20 h. Subsequently, through a secondary leaching process using a 3 mol/L solution of either HNO_3 or HCl, more than 95 % of Mn was leached from

the leaching residue. This stepwise leaching approach offers a clear pathway and favorable conditions for subsequent processing and recovery operations.

It can be observed that the optimization results in this study were based on single-factor experiments. In future studies, more advanced test design methods, such as response surface methodology (RSM) or factorial design, will be employed to systematically evaluate parameter interactions and optimize the process conditions. These approaches will enhance the statistical robustness of the results and further validate the scalability and applicability of the proposed method.

3.2. Solvent extraction of Mn

Bis(2-ethylhexyl) phosphoric acid (D2EHPA) P204 has previously been studied for Mn separation [5,27,34], and the general extraction mechanisms can be expressed as in **Eq. (1)**.

$$M^{2+} + 2\overline{(HA)_2} \rightleftarrows \overline{MA_4H_2} + 2H^+ \quad (1)$$

where M represents the metals, $(HA)_2$ represents D2EHPA in the organic phase, and MA_4H_2 represents the organic complex.

The distribution ratio of the extraction and the efficiency of metal extraction was determined by **Eq. (2)** and **Eq. (3)**:

$$D = \frac{C_{org}}{C_{aq}} \quad (2)$$

$$\%E = 100 \times \frac{D}{D + (V_{aq}/V_{org})} \quad (3)$$

The equation could be also expressed as in **Eq. (4)**,

$$logD = logK + 2\log[HX] - 2\log[H^+] \quad (4)$$

3.2.1. Effect of the contact time and aqueous phase pH

The effect of the initial pH levels of the aqueous solution (1.0, 2.0, 3.0, and 4.0) on Mn extraction was investigated. The aqueous phase was sampled after different contact times (1, 3, 5, 8, 10, 15, 20, and 30 min).

As illustrated in Fig. 9, it is evident that extraction time significantly impacts Mn extraction. Under all pH conditions, the efficiency and rate of manganese extraction were high within the initial 5 min. As the extraction time increased, the extraction rate gradually decreased due to the decreasing concentration difference and saturation of the extractant. Based on the data from both HCl and HNO_3 leachates, pH significantly affects Mn extraction efficiency using D2EHPA. In the HCl leachate, extraction rates at 15 mins increased from 33.5 % at pH 1.0 to 98.8 % at pH 4.0. Similarly, for the HNO_3 leachates, rates increased from 36.1 % at pH 1.0 to 99.1 % at pH 4.0. These findings highlight the enhanced affinity of Mn towards D2EHPA with an increasing initial pH. Additionally, the extraction efficiency for Mn was slightly higher in the HNO_3 leachate compared to the HCl leachate at equivalent pH levels. Kinetic analysis indicated a rapid initial rise in the extraction rate, stabilizing after 5 min. For optimal Mn extraction, a pH of 4.0 with a contact time of 5 min is recommended.

3.2.2. Effect of the extractant concentration

The effect of the extractant concentration (0.1–1.0 mol/L) on Mn extraction was investigated using an initial pH of 4.0 and a contact time of 5 min at ambient temperature. As presented in Fig. 10, higher extractant concentrations led to a greater manganese extraction efficiency. Specifically, as illustrated in Fig. 10**b**, at a concentration of 0.1 mol/L, the manganese extraction rate after 5 min was 68.4 %, with a Mn concentration of 5,500 ppm in the aqueous phase. When the concentration increased to 0.5 mol/L, the extraction rate rose to 99.1 % within 5 min, with the Mn concentration decreasing to roughly 280 ppm. At a concentration of 1.0 mol/L, the extraction rate further increased to 99.5 %, with the Mn concentration decreasing to 70 ppm. The increased entry of Mn into the organic phase is attributed to the higher extractant concentration, which enhances the probability of collision between extractant molecules and metal ions, providing more coordination sites for Mn complexation.

By plotting the logarithm of the P204 concentration against the logarithm of the distribution ratio using **Eq. (4)**, the number of extractant molecules involved in extracting a Mn^{2+} ion was determined. According to the results, the slope of the linear equation is close to 2, confirming that the extraction of each Mn^{2+} ion requires two extractant molecules. This finding is consistent with results of [13] regarding the selective extraction of Mn from waste lithium-ion batteries.

Based on the aforementioned observations, the optimal conditions for the Mn extraction system are as follows: 0.5 mol/L D2EHPA as the extractant, an aqueous solution with a pH of 4.0, a contact time of 5 min, and ambient temperature. These conditions apply to both HCl and HNO_3 leachates. Under these optimized extraction parameters, over 99 % of Mn ions in the leachates are extracted with high selectivity and efficiency, priming them for subsequent treatment steps.

3.2.3. Mn stripping

The impact of different stripping agents on Mn stripping was preliminarily explored using the method of controlled variables. The stripping agents used were as follows: distilled water, sodium chloride (NaCl, 1.0 mol/L), sodium nitrate ($NaNO_3$, 1.0 mol/L), hydrochloric acid (HCl, 1.0 mol/L), nitric acid (HNO_3, 1.0 mol/L), and sulfuric acid

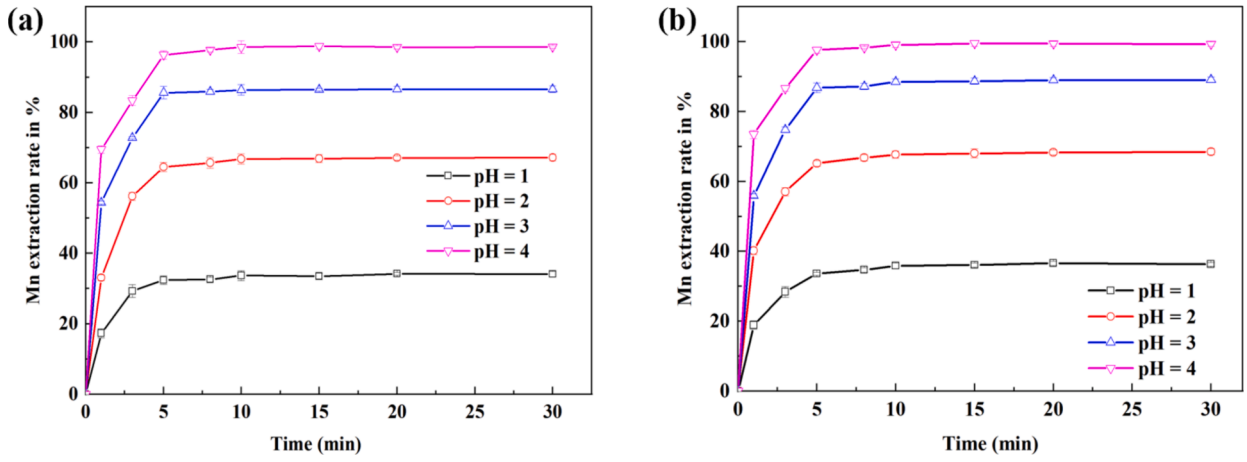

Fig. 9. Effect of the initial pH of the aqueous solution of (a) HCl and (b) HNO_3 (1 M D2EHPA with O:A = 1:1 at ambient temperature). Standard deviation based on triplicate tests.

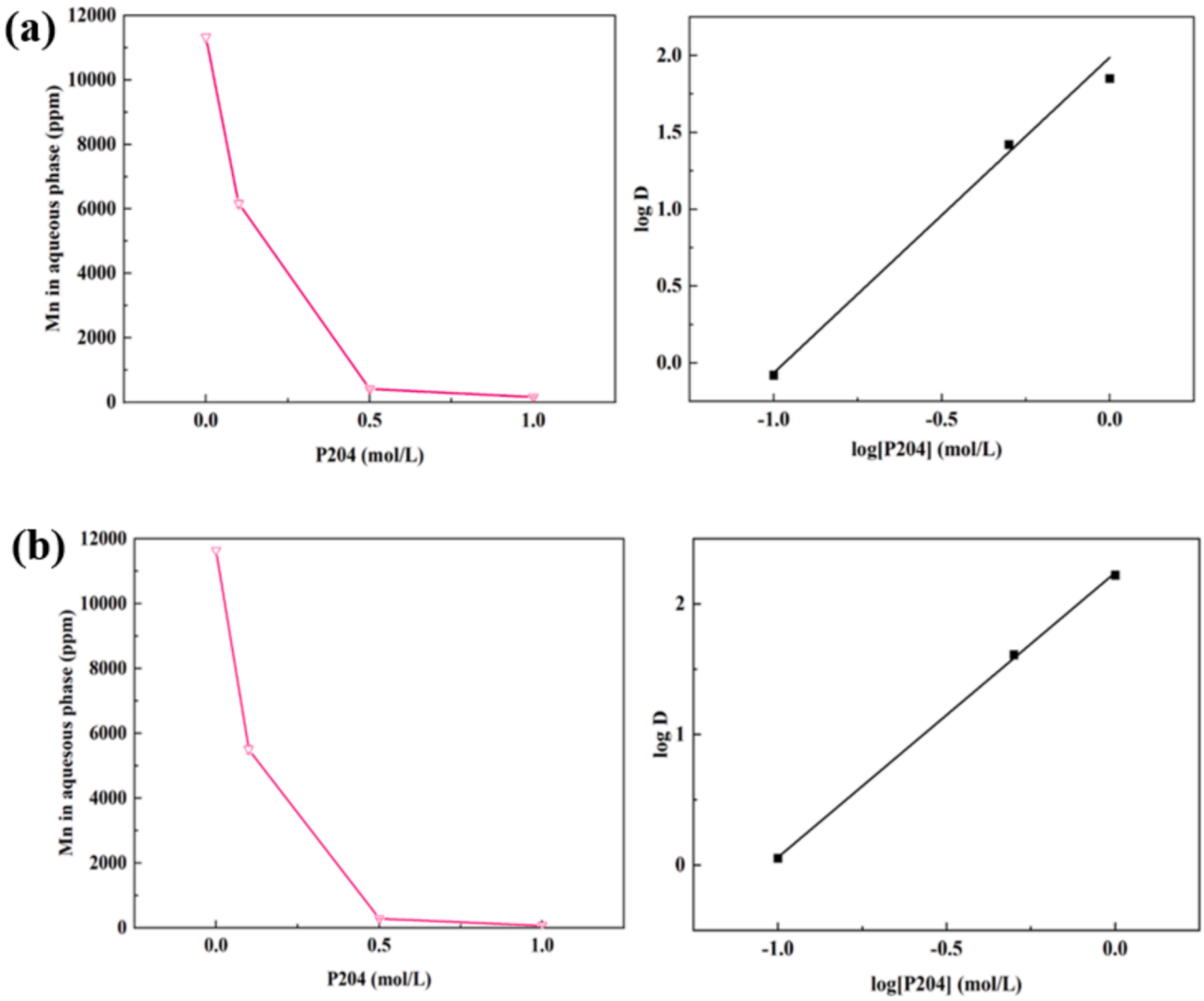

Fig. 10. Effect of the extractant concentration on Mn extraction from (a) HCl and (b) HNO_3 solution leachate. Standard deviation based on triplicate tests.

(H_2SO_4, 0.5 mol/L). The experiments were conducted at ambient temperature with an organic-to-aqueous phase ratio (O/A) of 1 and a stripping time of 5 min, with the experimental results presented in the form of distribution ratios in Table 3.

Taking data for treatment of the organic phase of HCl leachateas an example, the stripping efficiencies of 1.0 mol/L NaCl and 1.0 mol/L $NaNO_3$ were 5.6 % and 3.7 %, respectively, suggesting that salt-based stripping agents exhibit low efficiency in Mn stripping. This is attributed to other substances in salt solutions competing with Mn ions for binding sites on the extractant, reducing the likelihood of Mn ions binding with the extractant, and thereby lowering the efficiency of Mn extraction. The stripping efficiency of Mn with distilled water was 75.8 %. In contrast to the inefficiency of salt-based stripping agents, 1.0 mol/L HCl and 1.0 mol/L HNO_3 displayed higher stripping efficiencies of 76.9 % and 81.3 %, respectively, indicating that acidic conditions favor effective Mn stripping. However, the stripping efficiency of 0.5 mol/L H_2SO_4 was as high as 89.3 %, further indicating the advantage of acidic environments, especially strong acidic environments, for Mn stripping.

Table 3
Distribution ratios (D) of Mn stripping after extraction using various agent.

	D_{Mn}) (Aq. phase from HCl solution)	D_{Mn} (Aq. phase from HNO_3 solution)
MQ Water	0.32 ± 0.01	0.34 ± 0.01
1.0 mol/L NaCl	17 ± 1.1	19 ± 1
1.0 mol/L $NaNO_3$	26 ± 1	30 ± 1
1.0 mol/L HCl	0.30 ± 0.02	0.29 ± 0.02
1.0 mol/L HNO_3	0.23 ± 0.01	0.22 ± 0.01
0.5 mol/L H_2SO_4	0.12 ± 0.01	0.11 ± 0.01

The data for treatment of the organic phase of HNO_3 leachatewere similar to those for the treatment of HCl leachate, with 0.5 mol/L H_2SO_4 exhibiting the highest stripping efficiency of 90 %. Therefore, H_2SO_4 solution was selected as the primary stripping agent for further research and optimization analysis.

The influence of the sulfuric acid (H_2SO_4) concentration (0.5 to 2.0 mol/L) on Mn stripping was investigated at ambient temperature with an O/A ratio of 1. To accurately capture the dynamic changes, reaction solutions were collected at 1, 3, 5, and 10 min for analysis to monitor the Mn stripping efficiency.

The results are presented in Fig. 11, illustrating that the stripping time significantly impacts the Mn stripping efficiency. Under all experimental concentrations, stripping from both HNO_3 and HCl leachates displayed noticeable rate variations. The stripping rate increased significantly within the first 5 min, then slowed as the time extended to 10 min. This slowdown was due to the reduction in extractable substances and the approach to equilibrium after the initial rapid stripping

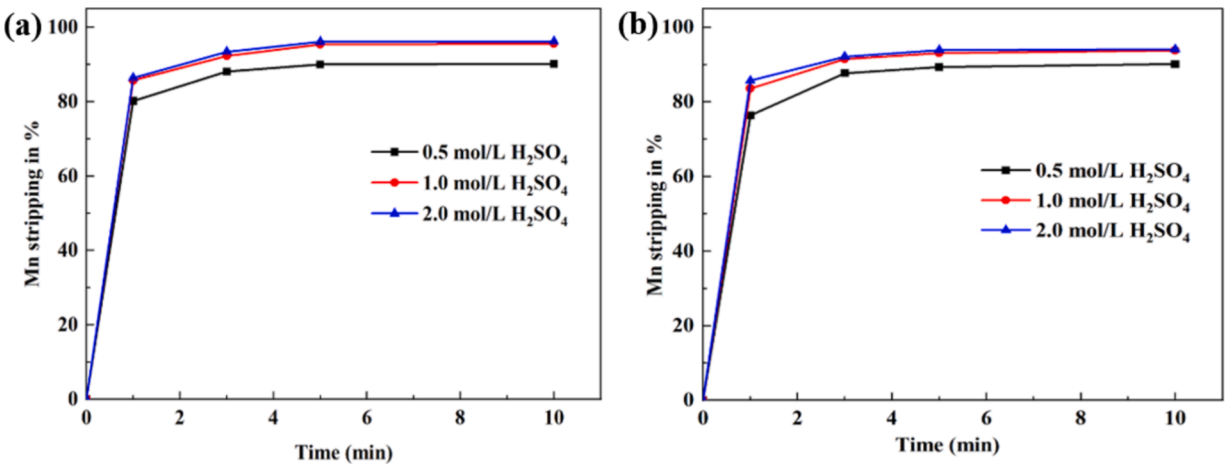

Fig. 11. The Mn stripping rate from the organic phase of (a) nitric acid leachate and (b) hydrochloric acid leachate using H_2 SO_4 solution.

phase. Extending the time slightly improved the stripping efficiency, but the gain decreased significantly. Therefore, the optimal stripping time is 5 min.

Fig. 11**a** illustrates that when stripping from nitric acid leachate, as the H_2SO_4 concentration increased from 0.5 mol/L to 2.0 mol/L, the stripping efficiency rose from 90.2 % to 96.8 %. Similarly, Fig. 11**b** shows that for the HCl leachate, the efficiency increased from 90.1 % to 94.4 %.

In conclusion, with an increase in the concentration of the stripping agent, the stripping efficiency also increases. This is because increasing the concentration of the stripping agent can alter the equilibrium distribution of the solute between the two phases, allowing more solute to enter the phase containing the stripping agent. Although the stripping efficiency of 2.0 mol/L H_2SO_4 was slightly higher than that of 1.0 mol/L H_2SO_4, a stripping agent concentration of 1.0 mol/L is recommended.

After the extraction procedure, Mn-enriched mono solutions were obtained through stripping with a 1.0 mol/L H_2SO_4 solution. The performance data for these extractions are detailed in Table 4. Regarding Mn recovery from HCl leachates, the extraction efficiency was 96.3 % and the stripping efficiency reached 93.1 %. In the case of HNO_3 leachates, both extraction and stripping efficiencies were slightly higher, being 97.6 % and 95.4 %, respectively. Overall, it can be deduced that approximately 90 % of the Mn from HCl leachates and 93 % from HNO_3 leachates was effectively recovered. A more detailed analysis of the extraction and recovery processes will be described in another article (unpublished).

3.3. As removal

In our prior investigation, the characterization outcomes of the HAP@$CoFe_2O_4$ composite were detailed [26](Fig. 12). Fig. 12**a** presents distinct X-ray diffraction peaks corresponding to the (201), (211), and (213) planes of hydroxyapatite, and the (220), (311), (400), (511), and (531) planes of cobalt ferrite, affirming the phase integrity of the composite. The crystallite size for $CoFe_2O_4$ was determined to be 10.60 nm, indicative of the nanocomposite's structural composition.

TEM analysis of HAP@$CoFe_2O_4$ revealed a bundle-like structure characteristic of hydroxyapatite, with nanoscale cobalt ferrite uniformly dispersed and tightly anchored on the surface. The Brunauer–Emmett–Teller (BET) surface area was measured at 12.2 m^2/g, indicating ample active sites for adsorption. The pore structure, characterized by the Barrett–Joyner–Halenda (BJH) method using N_2 adsorption/desorption isotherms, showed an average pore diameter of 15.3 nm, indicative of a slit-pore geometry within the composite material.

Table 4
The yield of recycled Mn from HCl and HNO_3 leachates. All results are presented as a percentage of the concentration in the leachates.

	HCl leachate	HNO_3 leachate
Extraction (%)	96.3 ± 1.2	97.6 ± 0.9
Stripping (%)	93.1 ± 0.3	95.4 ± 0.8
Total (%)	89.7 ± 1.4	93.1 ± 1.6

The synthesis of HAP@$CoFe_2O_4$ resulted in a material with a uniform compositional distribution and a narrow particle size range. These nanoparticles are well suited for use as an adsorbent in the decontamination of As from leaching effluents.

Based on the experimental data (as presented in Fig. 13), the influence of leachate pH and contact time on the adsorption efficiency of arsenic using HAP@$CoFe_2O_4$ (dosage 1.0 g/L) was systematically investigated. The adsorption efficiency significantly increased with an increase in pH from 2.0 to 7.0. Rapid adsorption was observed between pH 4.0 and 6.0, indicating an optimal range for arsenic adsorption. However, a slight reduction in efficiency occurred at pH 8.0, probably due to adverse effects on adsorption sites or other chemical interactions [19].

Regarding the impact of contact time, an initial rapid uptake of As was evident within the first 5 min across all pH levels, followed by a gradual approach to equilibrium. For most pH conditions, equilibrium was attained with a contact time between 5 and 10 min, indicating that a relatively short time is required for the adsorption process to stabilize.

Considering these findings, pH values of 6.0 and 7.0 emerged as the most favorable conditions, achieving over 93 % adsorption within just 5 mins. Thus, under the defined experimental parameters, an aqueous pH of 6.0 or 7.0 coupled with a contact time of 5 min is recommended for optimal As adsorption.

Upon examining the adsorption data for As removal from NaOH leachates using HAP@$CoFe_2O_4$, it is clear that the adsorbent dosage significantly affects the efficiency of the process. As the dosage increased from 1.0 g/L to 5.0 g/L, the adsorption efficiency rose substantially. At 1.0 g/L, the efficiency peaked at 94.1 %, while at 5.0 g/L, it reached 99.7 % and then slightly improved to 99.8 %. This improvement indicates that higher dosages provide more active sites for adsorption. Additionally, a rapid increase in adsorption efficiency was observed within the first 5 min for all dosages, stabilizing thereafter as equilibrium was approached. Thus, the optimal conditions for As adsorption are achieved at pH 7.0, with a 5.0 g/L dosage of HAP@$CoFe_2O_4$ and a contact time of at least 5 min at ambient temperature.

It should be noted that all the adsorption results were obtained in a solution with various other competing elements, making it challenging to isolate parameters such as the theoretical highest adsorption capacity

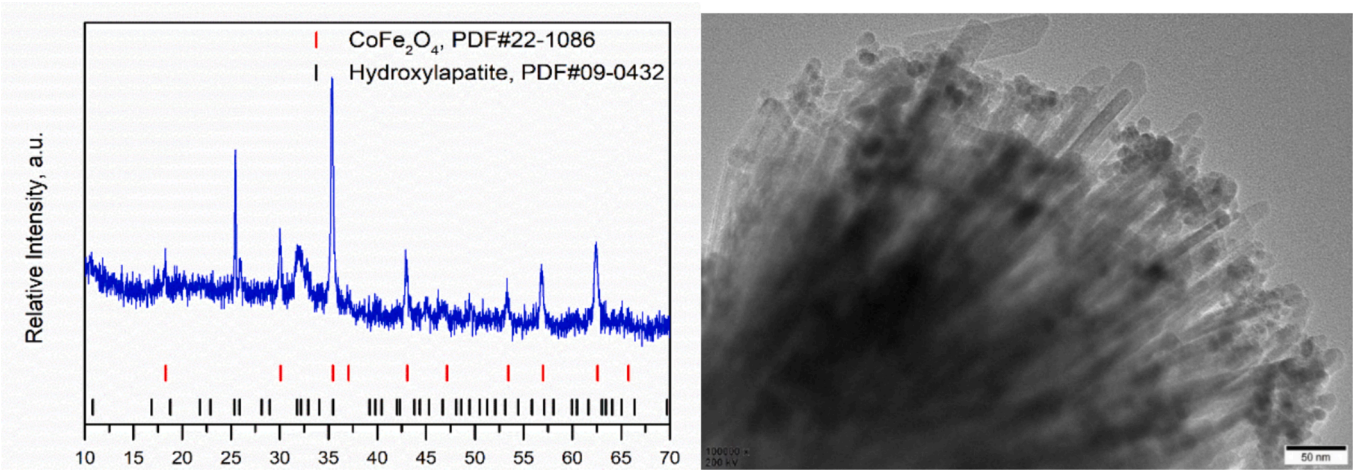

Fig. 12. (a) XRD analysis diagram of the crystal structure of HAP@$CoFe_2$ O_4. (b) TEM characterization of the microscopic morphology of HAP@$CoFe_2$ O_4.

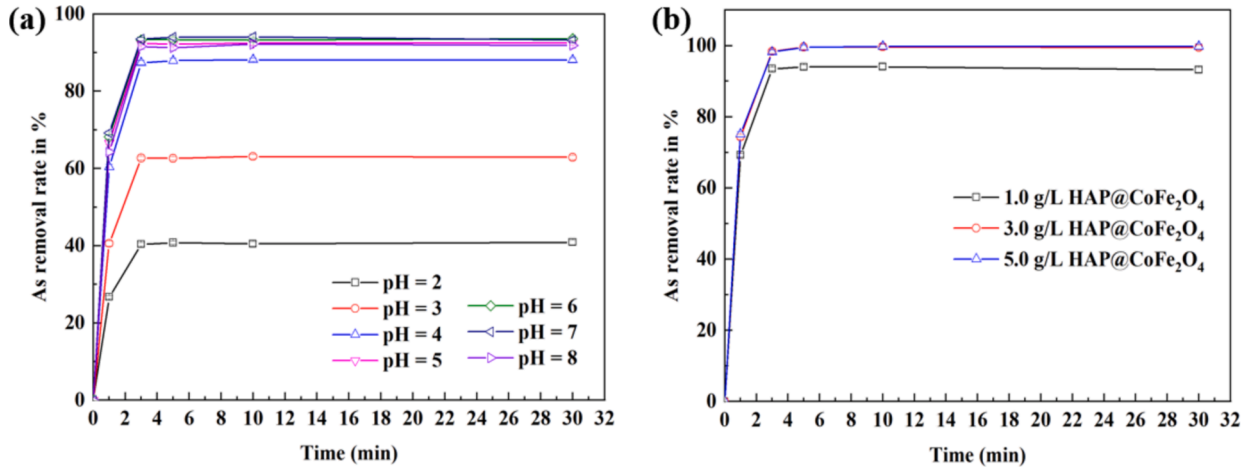

Fig. 13. (a) Effect of the initial pH value of the effluent solution on As removal from the effluent (with a dosage of 1.0 g/L at ambient temperature). (b) Effect of the adsorbent dosage on As removal from the effluent (with a solution pH value of 7.0 at ambient temperature). Standard deviation based on triplicate tests.

(q_m), isotherm constant, and kinetic constant. These parameters should be further evaluated in controlled experiments using mono-element artificial solutions.

3.4. *Suggested flowsheet and potential effect*

The proposed flowsheet for Mn recovery and As removal from manganese waste residue is depicted in Fig. 14. This streamlined process comprises two distinct leaching stages, Mn extraction and As adsorption. Initially, nearly all As is selectively leached using 3 mol/L NaOH at ambient temperature over 20 h with an L/S ratio of 10, yielding Reffinate I. Subsequently, approximately 95 % of Mn is extracted using either 3 mol/L HNO_3 or HCl, producing Reffinate II.

For Mn recovery from Reffinate II, 1 mol/L D2EHPA (P204) facilitates extraction, followed by stripping with 1 mol/L H_2SO_4. Operating at an O:A ratio of 1:1 for 5 min, an enriched mono Mn solution with over 95 % purity is obtained. The organic phase, or extractant, is recyclable post-purification. Regarding As in Reffinate I, it is effectively adsorbed using HAP@$CoFe_2O_4$. Optimal conditions include a pH of 7.0, an adsorbent dosage of 5.0 g/L, and a contact time of 5 min.

In laboratory-scale tests, this integrated approach achieves high efficiencies in both Mn recovery and As removal, suggesting its potential for upscale and broader applications. For As removal, such as chemical precipitation and adsorption using activated carbon, often face challenges including high chemical consumption, secondary pollution, and reduced selectivity in the presence of competing ions [19]. In contrast, the use of HAP@$CoFe_2O_4$ in our study achieved a remarkable As removal rate of 99.8 % within just 10 mins, coupled with the advantage of magnetic separation, which simplifies operations and lowers costs. Similarly for Mn recovery, such as direct leaching with strong acids result in significant waste generation and higher operational costs [17]. Our integrated approach, combining selective leaching, solvent extraction with D2EHPA, and optimized stripping, not only achieved a Mn recovery rate of 93.1 % but also minimized secondary waste production. These results underscore the dual benefits of enhanced efficiency and alignment with sustainable development principles and will have significant impacts on various stakeholders.

Implementing a novel technology for the harmless treatment of and resource recovery from Mn slag presents various benefits for key stakeholders (Table 5). For the local community and residents, the technology promises improved environmental quality by reducing soil and groundwater pollution, thereby enhancing their quality of life and health. However, short-term disruptions during construction and potential environmental risks must be managed effectively. Government and regulatory agencies can benefit from improved compliance with environmental regulations and enhanced public health. However, they face the challenge of allocating resources for monitoring and managing potential public trust issues if the technology underperforms. Mining

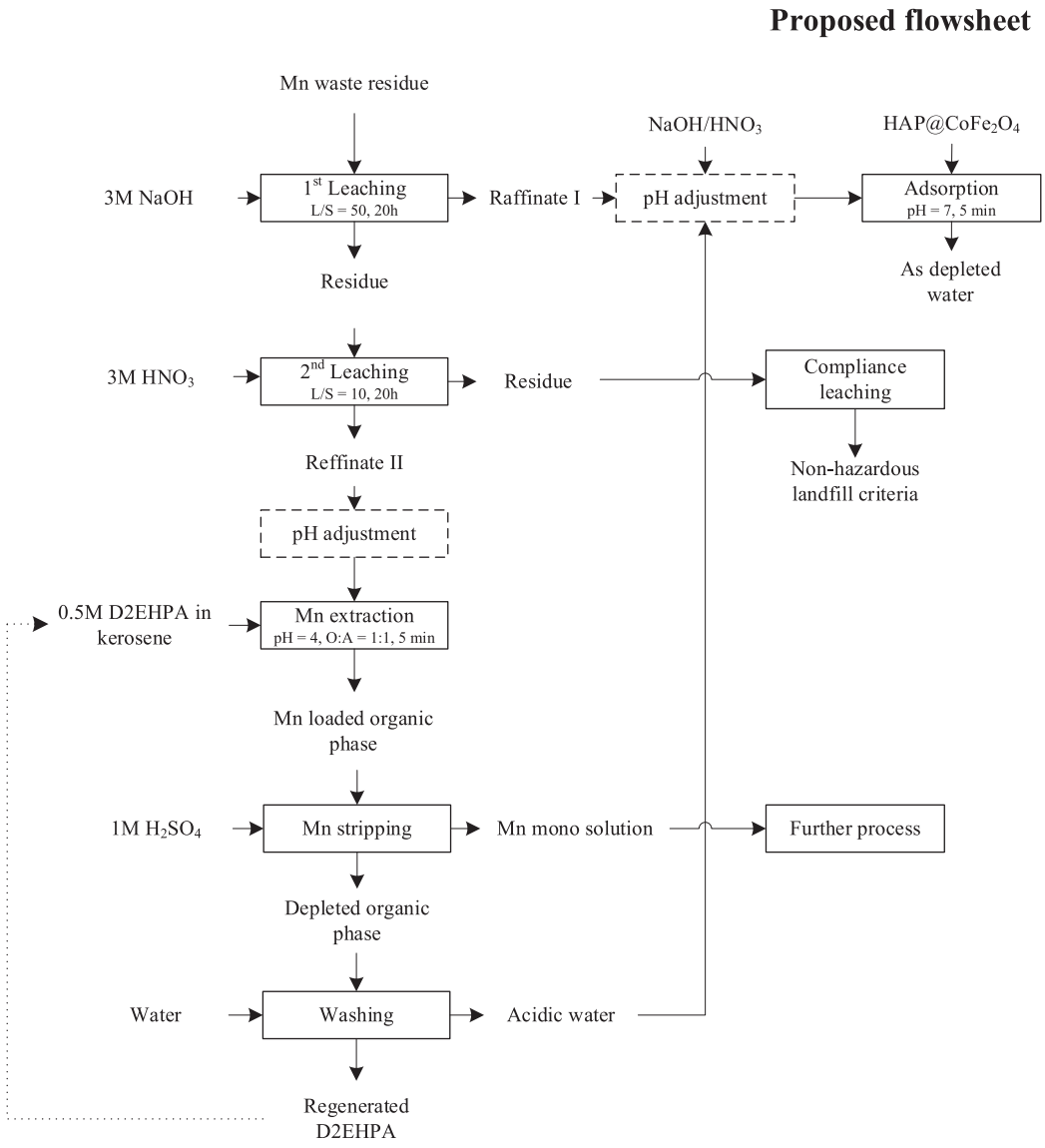

Fig. 14. Schematic diagram of the proposed flowsheet for Mn recovery and As decontamination from Mn slag.

companies stand to gain from reduced slag treatment costs, improved resource utilization, and an enhanced corporate image, although they must navigate the high initial investment costs and implementation risks. Environmental organizations and the public will see a promotion of environmental protection efforts and increased public awareness but may harbor skepticism about the technology's effectiveness, potentially increasing resistance to the project. Research institutions and universities can benefit from new research opportunities, strengthened collaboration between industry and academia, and funding for further research. However, they face challenges in applying research results and maintaining their reputation if the project fails. Lastly, downstream industrial supply chain enterprises could experience reduced raw material costs and improved production efficiency, along with a stable supply of manganese resources. However, they must contend with the potential impacts on production processes due to unstable raw material quality and increased supply chain risks associated with the new materials.

In summary, adopting this innovative technology for Mn slag treatment and resource recovery holds substantial promise for environmental, economic, and societal benefits. However, its successful implementation and sustainability require careful management of potential risks and active stakeholder engagement. While the potential impacts on stakeholders discussed above provide valuable insights, they are based on qualitative analysis and represent possible effects of the proposed approach. A more comprehensive evaluation of environmental risks and economic feasibility necessitates the support of scientific methodologies and actual data. Future studies will address these gaps by scaling up the experiments, collecting relevant datasets, and employing robust tools such as Monte Carlo simulations and IPCC frameworks to deliver a detailed and reliable assessment of the technology's practical applications.

4. Conclusion

In this study, the critical environmental challenge of manganese and arsenic pollution from Mn slag in a mining area in China was addressed. A novel approach was introduced, comprising selective leaching, solvent extraction, and adsorption, providing a comprehensive solution for Mn recovery and associated As decontamination.

The outcomes of the study highlight the distinct leaching behaviors of Mn and As, with over 98 % of As and 95 % of Mn successfully and sequentially extracted under optimal conditions. A notable Mn extraction rate of 93.1 % was achieved from the HNO_3 leachate solution using di(2-ethylhexyl) phosphoric acid (D2EHPA) in the solvent extraction phase. The resulting enriched Mn mono solution offers significant

Table 5
Positive and negative impacts on potential stakeholders.

Potential targets	Pros.	Cons.
Local community and residents	1. Reduction in environmental pollution. 2. Benefits from cleaner water resources and a safer living environment. 3. Improved quality of life and health.	1. Uncertainty. For instance, potential operational risks associated with new technology. 2. Potential public dissatisfaction.
Government and regulatory agencies	1. Compliance with environmental protection regulations and policy goals. 2. Improved regional environmental conditions and public health. 3. Enhanced government credibility and public satisfaction.	1. Increased resource allocation for regulation and monitoring. 2. Potential public trust issues if the technology fails.
Mining companies	1. Improved corporate image and alignment with sustainable development strategies. 2. Increased profit sources and enhanced competitiveness.	1. High initial investment costs, increasing economic burden. 2. Uncertainty risks during implementation of the technology.
Downstream industrial supply chain enterprises	1. Reduced raw material costs and improved production efficiency. 2. Increased supply of manganese resources, ensuring stable production. 3. Promotion of green manufacturing, enhancing product competitiveness.	1. Potential impact on production processes due to unstable raw material quality. 2. Increased supply chain risks due to reliance on new materials.
Environmental organizations and the public	1. Promotion of environmental technology applications and environmental protection efforts. 2. Increased public environmental awareness and participation.	1. Potential skepticism about the treatment process and outcomes, increasing project resistance.
Research institutions and universities	1. Provides research topics and opportunities for application of the technology. 2. Strengthened research collaboration between industry and academia, promoting technology transfer and dissemination. 3. Secured government and corporate funding, enhancing research capabilities.	1. Technical bottlenecks and challenges during the application of research results.

potential for further recovery and reuse in various industrial applications.

Additionally, the magnetically separable nano-hydroxyapatite@cobalt ferrite (HAP@$CoFe_2O_4$) adsorbent was highly effective, eliminating 99.8 % of As from the leaching effluent in under 10 min. This efficiency underscores the potential of HAP@$CoFe_2O_4$ as a reliable solution for As sequestration. Furthermore, HAP@$CoFe_2O_4$ was efficiently recycled via an external magnetic field, thereby reducing costs and simplifying subsequent treatment and disposal processes, ultimately decreasing environmental pollution.

Overall, this study not only introduces an efficient method for Mn and As extraction and removal but also emphasizes the potential avenues for resource recovery. Based on the experimental results, the proposed process, including leaching, extraction, and consequential decontamination, could be a promising strategy for Mn slag disposal and reclamation.

Future investigations should focus on the competitive and selective adsorption of other metal ions in leachates. Additionally, the subsequent processes for the final by-products, including used HAP, leaching residue, and effluent, require a thorough examination. A strict evaluation of effluent emissions must be conducted to address other contaminants present. Furthermore, detailed assessments of both economic viability and environmental impacts are planned to ensure a comprehensive understanding and optimization of the process.

Declaration of generative AI and AI-assisted technologies in the writing process

During the preparation of this work, the authors used ChatGPT to polish the English language. After using this tool/service, the authors reviewed and edited the content as needed and take full responsibility for the content of the published article.

CRediT authorship contribution statement

Jinfeng Tang: Conceptualization, Writing – original draft, Supervision, Resources, Funding acquisition. **Qian Feng:** Methodology, Investigation, Formal analysis. **Xiangqin Peng:** Data curation, Formal analysis. **Lizhi Tong:** Methodology, Data curation, Formal analysis, Writing – original draft. **Jianzhao Wu:** Methodology, Data curation. **Xinmei Lin:** Investigation, Formal analysis. **Lezhang Wei:** Methodology, Writing – review & editing. **Minhua Su:** Writing – review & editing. **Kaimin Shih:** Methodology, Writing – review & editing. **Małgorzata Szlachta:** . **Junhua Xu:** Funding acquisition, Methodology, Writing – review & editing.

Declaration of competing interest

The authors declare that they have no known competing financial interests or personal relationships that could have appeared to influence the work reported in this paper.

Acknowledgments

This work was supported by the National Natural Science Foundation of China (No. 22076034), the Natural Science Foundation of Guangdong Province, China (No. 2023A0505050143), the Famous Overseas Teachers Project of Guangdong Province, China (2022) and the mineral and materials technology project (5040880011) of Geological Survey of Finland.

Data availability

Data will be made available on request.

References

[1] A. Alengebawy, S.T. Abdelkhalek, S.R. Qureshi, M.-Q. Wang, Heavy metals and pesticides toxicity in agricultural soil and plants, Ecol. Risks Human Health Implicat. Toxics. (2021).
[2] Q. Bei, T. Yang, C. Ren, E. Guan, Y. Dai, D. Shu, W. He, H. Tian, G. Wei, Soil pH determines arsenic-related functional gene and bacterial diversity in natural forests on the Taibai Mountain, Environ. Res. 220 (2023), 115181.
[3] H. Chen, Y. Gao, H. Dong, B. Sarkar, H. Song, J. Li, N. Bolan, B.F. Quin, X. Yang, F. Li, F. Wu, J. Meng, H. Wang, W. Chen, Chitin and crawfish shell biochar composite decreased heavy metal bioavailability and shifted rhizosphere bacterial community in an arsenic/lead co-contaminated soil, Environ. Int. 176 (2023), 107989.
[4] L. Chen, M. Zhou, J. Wang, Z. Zhang, C. Duan, X. Wang, S. Zhao, X. Bai, Z. Li, Z. Li, L. Fang, A global meta-analysis of heavy metal(loid)s pollution in soils near copper mines: evaluation of pollution level and probabilistic health risks, Sci. Total Environ. 835 (2022), 155441.

[5] P.K. Choubey, O.S. Dinkar, R. Panda, A. Kumari, M.K. Jha, D.D. Pathak, Selective extraction and separation of Li, Co and Mn from leach liquor of discarded lithium ion batteries (LIBs), Waste Manag. 121 (2021) 452–457.
[6] S. Dey, B. Tripathy, M.S. Kumar, A.P. Das, Ecotoxicological consequences of manganese mining pollutants and their biological remediation, Environ. Chem. Ecotoxicol. 5 (2023) 55–61.
[7] P.P. Esfahani, M. Mahdavinia, L. Khorsandi, M. Rezaei, H. Nikravesh, M. J. Khodayar, Betaine protects against sodium arsenite-induced diabetes and hepatotoxicity in mice, Environ. Sci. Pollut. Res. 30 (4) (2023) 10880–10889.
[8] W. Feng, X. Xiao, J. Li, Q. Xiao, L. Ma, Q. Gao, Y. Wan, Y. Huang, T. Liu, X. Luo, S. Luo, G. Zeng, K. Yu, Bioleaching and immobilizing of copper and zinc using endophytes coupled with biochar-hydroxyapatite: Bipolar remediation for heavy metals contaminated mining soils, Chemosphere 315 (2023), 137730.
[9] J. Guo, C. Yuan, Z. Zhao, Q. He, H. Zhou, M. Wen, Soil washing by biodegradable GLDA and PASP: Effects on metals removal efficiency, distribution, leachability, bioaccessibility, environmental risk and soil properties, Process Saf. Environ. Prot. 158 (2022) 172–180.
[10] Z. He, L. Long, H. Yuan, H. Pang, Y. Wang, L. Ye, M. Xu, C. Chen, Y. Liu, Y. Xiao, C. Xu, J. Wu, G. Yang, Remediation of heavy-metal-contaminated soil with two organic acids: Washing efficiency, recovery performance, and benefit analysis, J. Clean. Prod. 393 (2023), 136235.
[11] M. Imran, M. Ashraf, A.R. Awan, Growth, yield and arsenic accumulation by wheat grown in a pressmud amended salt-affected soil irrigated with arsenic contaminated water, Ecotoxicol. Environ. Saf. 224 (2021), 112692.
[12] M. Jiang, K. Wang, Y. Wang, Q. Zhao, W. Wang, Technologies for the cobalt-contaminated soil remediation: A review, Sci. Total Environ. 813 (2022), 151908.
[13] A. Keller, M.W. Hlawitschka, H.J. Bart, Application of saponified D2EHPA for the selective extraction of manganese from spend lithium-ion batteries, Chem. Eng. Process. - Process Intesif. 171 (2022), 108552.
[14] A. Komaei, A. Noorzad, P. Ghadir, Stabilization and solidification of arsenic contaminated silty sand using alkaline activated slag, J. Environ. Manage. 344 (2023), 118395.
[15] X. Li, W. Jiao, R. Xiao, W. Chen, W. Liu, Contaminated sites in China: countermeasures of provincial governments, J. Clean. Prod. 147 (2017) 485–496.
[16] Y. Li, X. Liao, W. Li, Combined sieving and washing of multi-metal-contaminated soils using remediation equipment: A pilot-scale demonstration, J. Clean. Prod. 212 (2019) 81–89.
[17] J. Liu, L. Zhao, Q. Liu, J. Li, Z. Qiao, P. Sun, Y. Yang, A critical review on soil washing during soil remediation for heavy metals and organic pollutants, Int. J. Environ. Sci. Technol. (2021) 1–24.
[18] Y. Liu, W. Cui, W. Li, S. Xu, Y. Sun, G. Xu, F. Wang, Effects of microplastics on cadmium accumulation by rice and arbuscular mycorrhizal fungal communities in cadmium-contaminated soil, J. Hazard. Mater. 442 (2023), 130102.
[19] A. Nayak, B. Bhushan, Hydroxyapatite as an advanced adsorbent for removal of heavy metal ions from water: Focus on its applications and limitations, Mater. Today Proc. 46 (2021) 11029–11034.
[20] T.V. Peres, M.R.C. Schettinger, P. Chen, F. Carvalho, D.S. Avila, A.B. Bowman, M. Aschner, Manganese-induced neurotoxicity: a review of its behavioral consequences and neuroprotective strategies, BMC Pharmacol. Toxicol. 17 (2016) 1–20.
[21] R. Praveen, R. Nagalakshmi, Review on bioremediation and phytoremediation techniques of heavy metals in contaminated soil from dump site, Mater. Today Proc. 68 (2022) 1562–1567.
[22] S. Rahman, I.M.M. Rahman, H. Hasegawa, Management of arsenic-contaminated excavated soils: a review, J. Environ. Manage. 346 (2023), 118943.
[23] X. Sheng, Z. Zhaohui, W. Zhihui, Effects of heavy metals on moss diversity and analysis of moss indicator species in Nancha manganese mining area, Southwestern China, Global Ecol. Conserv. 28 (2021) e01665.
[24] Q. Shi, M. Su, G. Yuvaraja, J. Tang, L. Kong, D. Chen, Development of highly efficient bundle-like hydroxyapatite towards abatement of aqueous U(VI) ions: Mechanism and economic assessment, J. Hazard. Mater. 394 (2020), 122550.
[25] Q. Su, Y. He, H. Pan, H. Liu, K. Mehmood, Z. Tang, L. Hu, Toxicity of inorganic arsenic to animals and its treatment strategies, Comp. Biochem. Physiol. C: Toxicol. Pharmacol. 271 (2023), 109654.
[26] J. Tang, S. Dong, Q. Feng, M. Su, Y. Wei, J. Liang, H. Zhang, L. Huang, L. Kong, N. Wang, E. Xiao, Y. Liu, X. Tang, T. Xiao, Optimizing critical metals recovery and correlative decontamination from MSWI fly ash: evaluation of an integrating two-step leaching hydrometallurgical process, J. Clean. Prod. 368 (2022), 133017.
[27] Vieceli, N., Reinhardt, N., Ekberg, C., Petranikova, M., 2021. Optimization of Manganese Recovery from a Solution Based on Lithium-Ion Batteries by Solvent Extraction with D2EHPA, Metals.
[28] N. Wang, H. Lu, B. Liu, T. Xiong, J. Li, H. Wang, Q. Yang, Enhancement of heavy metals desorption from the soil by eddy deep leaching in hydrocyclone, J. Environ. Sci. 135 (2024) 242–251.
[29] X. Wang, C. Zhang, B. Qiu, U. Ashraf, R. Azad, J. Wu, S. Ali, Biotransfer of Cd along a soil-plant- mealybug-ladybird food chain: a comparison with host plants, Chemosphere 168 (2017) 699–706.
[30] W.-Y. Xia, Y.-J. Du, F.-S. Li, G.-L. Guo, X.-L. Yan, C.-P. Li, A. Arulrajah, F. Wang, S. Wang, Field evaluation of a new hydroxyapatite based binder for ex-situ solidification/stabilization of a heavy metal contaminated site soil around a Pb-Zn smelter, Constr. Build. Mater. 210 (2019) 278–288.
[31] K. Yan, H. Wang, Z. Lan, J. Zhou, H. Fu, L. Wu, J. Xu, Heavy metal pollution in the soil of contaminated sites in China: Research status and pollution assessment over the past two decades, J. Clean. Prod. 373 (2022), 133780.
[32] J. Yang, R. Hu, C. Zhao, L. Wang, M. Lei, G. Guo, H. Shi, X. Liao, T. Chen, Challenges and opportunities for improving the environmental quality of cadmium-contaminated soil in China, J. Hazard. Mater. 445 (2023), 130560.
[33] H. Zhang, X. Yuan, T. Xiong, H. Wang, L. Jiang, Bioremediation of co-contaminated soil with heavy metals and pesticides: Influence factors, mechanisms and evaluation methods, Chem. Eng. J. 398 (2020), 125657.
[34] W. Zhang, C.Y. Cheng, Manganese metallurgy review. Part I: Leaching of ores/secondary materials and recovery of electrolytic/chemical manganese dioxide, Hydrometall. 89 (3) (2007) 137–159.
[35] N. Zheng, L. Yin, M. Su, Z. Liu, D.C. Tsang, D. Chen, Synthesis of shape and structure-dependent hydroxyapatite nanostructures as a superior adsorbent for removal of U (VI), Chem. Eng. J. 384 (2020), 123262.